Effective Date: 09/16/2024
Expiration Date: 09/16/2029

XRISM/ Resolve
CMO
09/18/2024
RELEASED

INSTRUMENT CALIBRATION REPORT

RESOLVE AND XTEND MIRROR VIGNETTING COEFFICIENTS

RESOLVE-SCI-RPT-0166

REVISION (A)

XRISM-XMA-CALDB-VIGNCOEF-407

X-ray Imaging and Spectroscopy Mission (XRISM) Project

NASA/GSFC Code 461

National Aeronautics and
Space Administration

Goddard Space Flight Center
Greenbelt, Maryland

Check https://ipdtdms.gsfc.nasa.gov
to verify that this is the correct version prior to use

Resolve and Xtend Mirror Vignetting Coefficients

Signature/Approval Page

Prepared by: Rozenn Boissay-Malaquin, Takayuki Hayashi, Keisuke Tamura, Takashi Okajima, Tahir Yaqoob, Megan E. Eckart

Reviewers/Approvers:

Megan Eckart
Takashi Okajima
Michael Lowenstein
Tahir Yaqoob

Approved by:

Megan Eckart

***** Electronic signatures are available on-line at: https://ipdtdms.gsfc.nasa.gov*****

Preface

This document is an XRISM Project signature-controlled document. Changes to this document require prior approval of the applicable Product Design Lead (PDL) or designee. Proposed changes shall be submitted in the Technical Data Management System (TDMS) via a Signature Control Request (SCoRe) along with supportive material justifying the proposed change. Changes to this document will be made by complete revision.

All of the requirements in this document assume the use of the word "shall" unless otherwise stated.

Questions or comments concerning this document should be addressed to:
XRISM Configuration Management Office
Mail Stop: 461
Goddard Space Flight Center
Greenbelt, Maryland 20771

Change History Log

Revision	Effective Date	Description of Changes (Reference the SCoRe Approval Date)
-	12/13/2023	Released per RESOLVE-SCoRe-0568 First two deliveries of vignetting coefficients based on ground calibration data.
A	09/16/2024	Released per RESOLVE-SCoRe-0573 Changed title page to "XRISM-XMA-CALDB-VIGNCOEF-407," updating " GEN" to "XMA" to match CalDB structure. No other changes.

NOTE to editors: The document name will be XRISM-CAL-RPT-XXXX, where XXXX is assigned by the TDMS system. The document will be cross-referenced in TDMS to the filename in the format XRISM-XXX-CALDB-FILEDESC-NN where XXX is the instrument or component (e.g. RESOLVE), FILEDESC refers to a specific calibration report (e.g., rmfparams) and NN the corresponding number assigned to that report by the SDC. For example the calibration report addressing the Resolve LSF calibration may be assigned XRISM-RESOLVE-CALDB-RMFPARAMS-01, that addressing the Resolve gain calibration XRISM-RESOLVE-GAINPIX-CALDB-02, etc. (where the numbers are to be provided by the SDC).

These documents are updated as needed, e.g. when the relevant CALDB files, or the relevant calibration data analysis, is revised. The document version will be assigned by the TDMS system. The tracking tool should be used to record changes.

This document must include the CalDB file name, an explanation of how the data were collected and the analysis conducted and, if using standard Ftools, the software version number. All revisions are consolidated into the same document to maintain a full record of all changes.

Table of Contents

1 Introduction

1.1 Purpose

This document describes how the data obtained during the ground calibration of the X-ray Mirror Assemblies (XMAs) for Resolve and Xtend instruments of the XRISM mission have been analyzed to create the vignetting coefficients CalDB file. This document also explains how the vignetting coefficients CalDB file is used by the software.

1.2 Scientific Impact

This CalDB file gives analytic approximations for XMA vignetting as a function of off-axis angle and X-ray energy. The coefficients for the analytic functions for Resolve and Xtend are stored in a single CalDB file. This CalDB file includes the vignetting information obtained during the ground calibration of the XMAs. It can, for example, be used as part of the process to convert observed images to flat-field images, which are more representative of intrinsic source flux. The vignetting coefficient file can be input to the tool *xaexpmap* to account for the XMA contribution to the distortion of intrinsic source flux. (Note that the flat-fielding functionality of *xaexpmap* is provided as an exploratory tool, whereas a more accurate approach is to construct models of the intrinsic spatial distribution in the image and use raytracing to compare simulated images with the data, in an iterative process.) The vignetting coefficients CalDB file can also be used by the *heasim* tool to simulate observation event files.

1.3 Description of the XMAs and their Ground Calibration

This document refers to ground calibration measurements that have been performed on both XMAs at NASA/GSFC. An overview of the XRISM mission, including a description of the XMAs, is presented in the XRISM Quick Reference document [1]. A full description of the ground calibration measurement setup and the XMAs performance is given in the papers by Boissay-Malaquin et al. 2022 [2], Tamura et al. 2022 [3], and Hayashi et al. 2022 [4].

1.4 Data Description

The ground calibration of both XMAs has been performed at the beamline located in NASA/GSFC. A detailed description of the measurement setup is given in Boissay-Malaquin et al. 2022 [2]. In particular, the definition of the mirror roll angle used for the ground calibration of the XMAs (different from the spacecraft roll angle) is illustrated in Figure 4 of the paper [2], and shown in more detail in the present document for clarification purposes (see Figure 1).

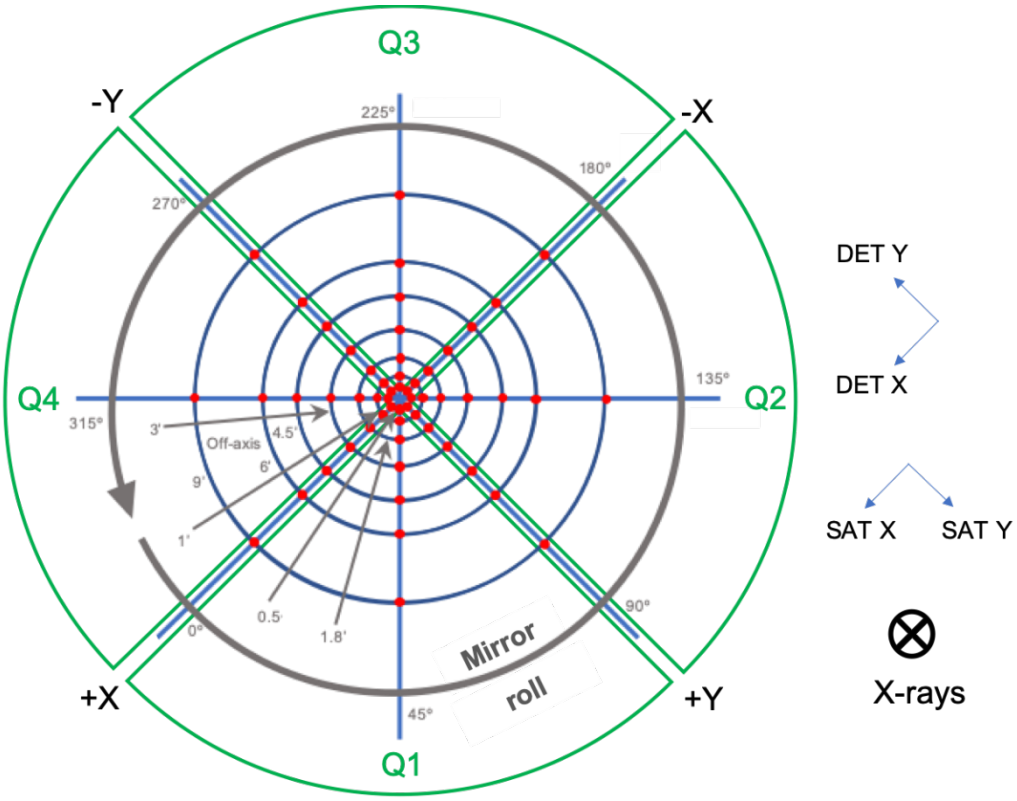

Figure 1: Look-down illustration of the mirror roll angle (different from the spacecraft roll angle) and the off-axis angle used during the ground calibration measurements (see Boissay-Malaquin et al. 2022 [2]). The coordinates of the satellite and detector are shown, as well as the boundaries of the XMAs' quadrants.

The effective area on-axis and off-axis has been measured at seven different energies. The full description of these vignetting measurements (i.e., measurements of effective area as a function of the off-axis angle) is given in Boissay-Malaquin et al. 2022 [2]. Figure 2 below summarizes the set of off-axis angles, mirror roll angles, and X-ray energies employed for the Resolve and Xtend XMA effective area measurements.

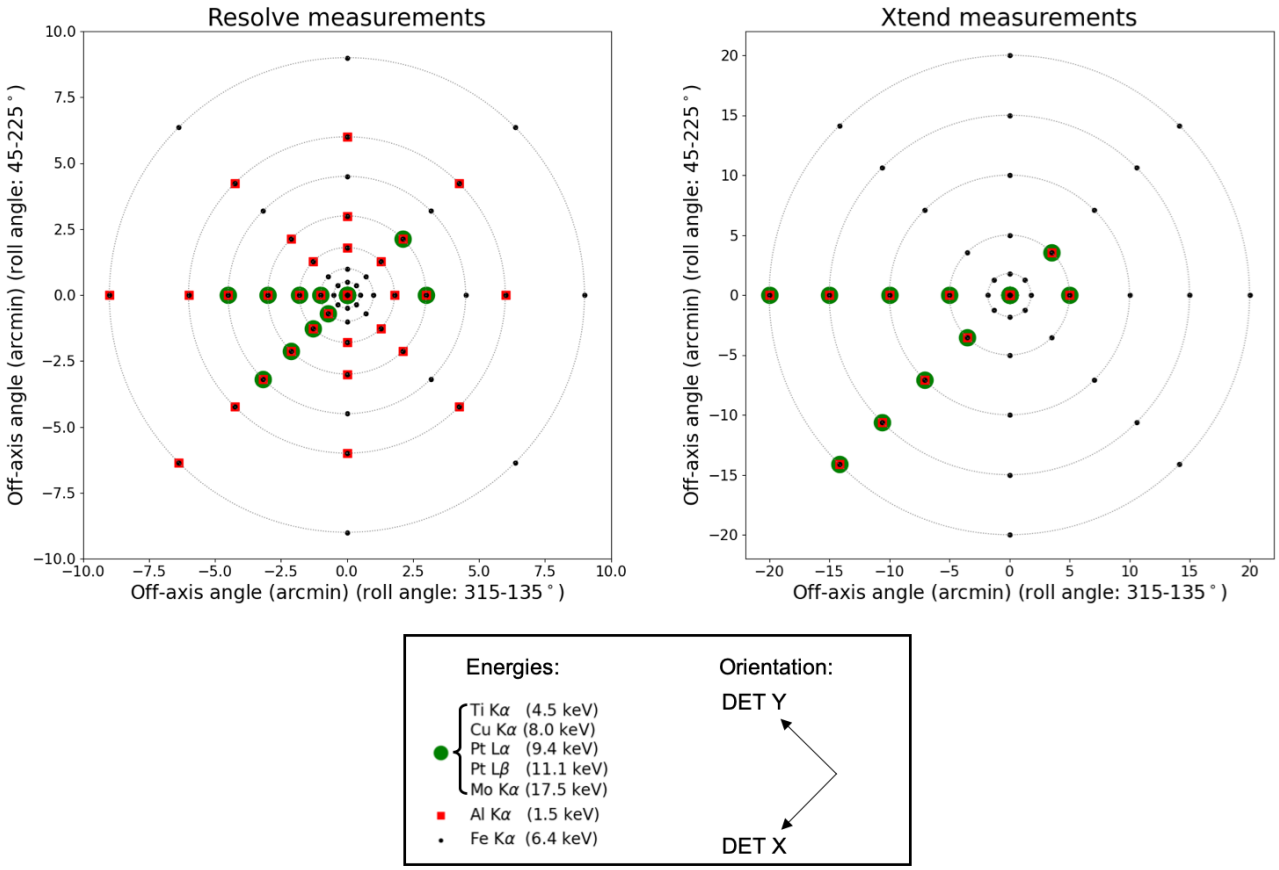

Figure 2: Points of measurement of the effective area at several off-axis and mirror roll angles, and at different energies, for Resolve (left) and Xtend XMAs (right). Note the different ranges of off-axis angles between both XMAs (from -9′ to 9′ for Resolve, and from -20′ to 20′ for Xtend). The orientation in this figure is the same as in Figure 1.

2 CalDB Release 20230615 (obsolete)

CalDB Filename	Validity date	File(s) as delivered	Delivery date	Comment
xa_gen_vigncoef_20190101v001	20190101 00:00 UT	FoV_fit.pdf	20230527	XMA vignetting coefficients to reproduce FWHM values

2.1 Data Analysis

We performed the data analysis using the *lmfit* least-square fitting method in Python. We show hereafter how we first fitted the vignetting curves at each energy, derived the corresponding Full

Width at Half Maximum (FWHM) of the model fitting the vignetting curves, and then modeled this FWHM as a function of energy.

2.1.1 Vignetting Curves

We fitted the effective area as a function of the off-axis angle (i.e. the vignetting curves), for each energy, with a combination of 2D Gaussian and Lorentzian models, for both XMAs. During the fitting process, we linked the center of the Gaussian and the Lorentzian models together. This fitting procedure is similar to the one used in Boissay-Malaquin et al. 2022 [2] for determining the optical axis at 6.4 keV.
The Field of View (FoV) is defined as the FWHM of the model fitting the vignetting curves. During the modeling of the vignetting curves, we linked the widths in the orthogonal directions defined by the mirror roll angles 315-135° and 45-225° (see Figure 1), in order to get only one value of FoV for all directions. These FoV values are then directly derived from the 2D fits with symmetrical models. An example of the measurement at 6.4 keV and its corresponding fit is shown in Figure 3 as an effective area map for Resolve XMA. In this figure, the effective area is measured at different off-axis angles and different mirror roll angles represented by the black dots, and the contours result from the interpolation of the effective area between these dots. An example of the projection of the effective area measurements at 6.4 keV and corresponding fits, in two different directions (centered on the XMAs' quadrants, and along the quadrants boundaries – see Figure 1), is shown in Figure 4, for both XMAs. As shown by the ratio of the measurements over the fitted model in Figure 4, the vignetting data at all energies are well reproduced by the combination of symmetrical and concentric Gaussian and Lorentzian models, for both Resolve and Xtend XMAs, in particular within +/-10′ of the optical axis.

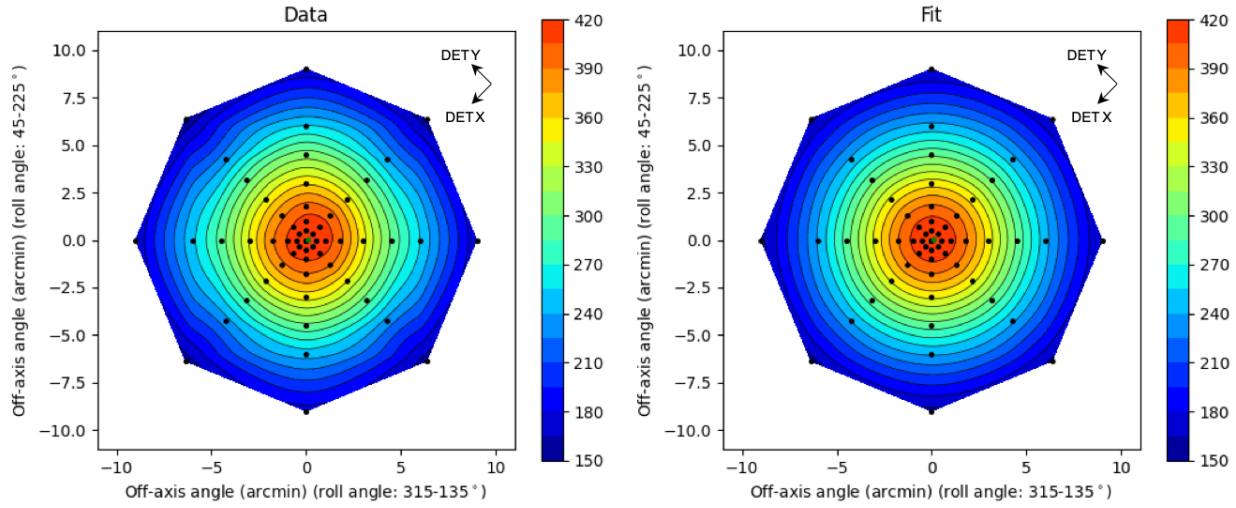

Figure 3: Effective area map from measurements at E=6.4keV (left) and 2D fit with the combination of Gaussian and Lorentzian models (right), for Resolve XMA. The black dots represent the measured off-axis angles, for different roll angles. The colors represent the value of the effective area (in cm^2), measured at these points and interpolated with the cubic method using the "griddata" function from the SciPy package in Python.

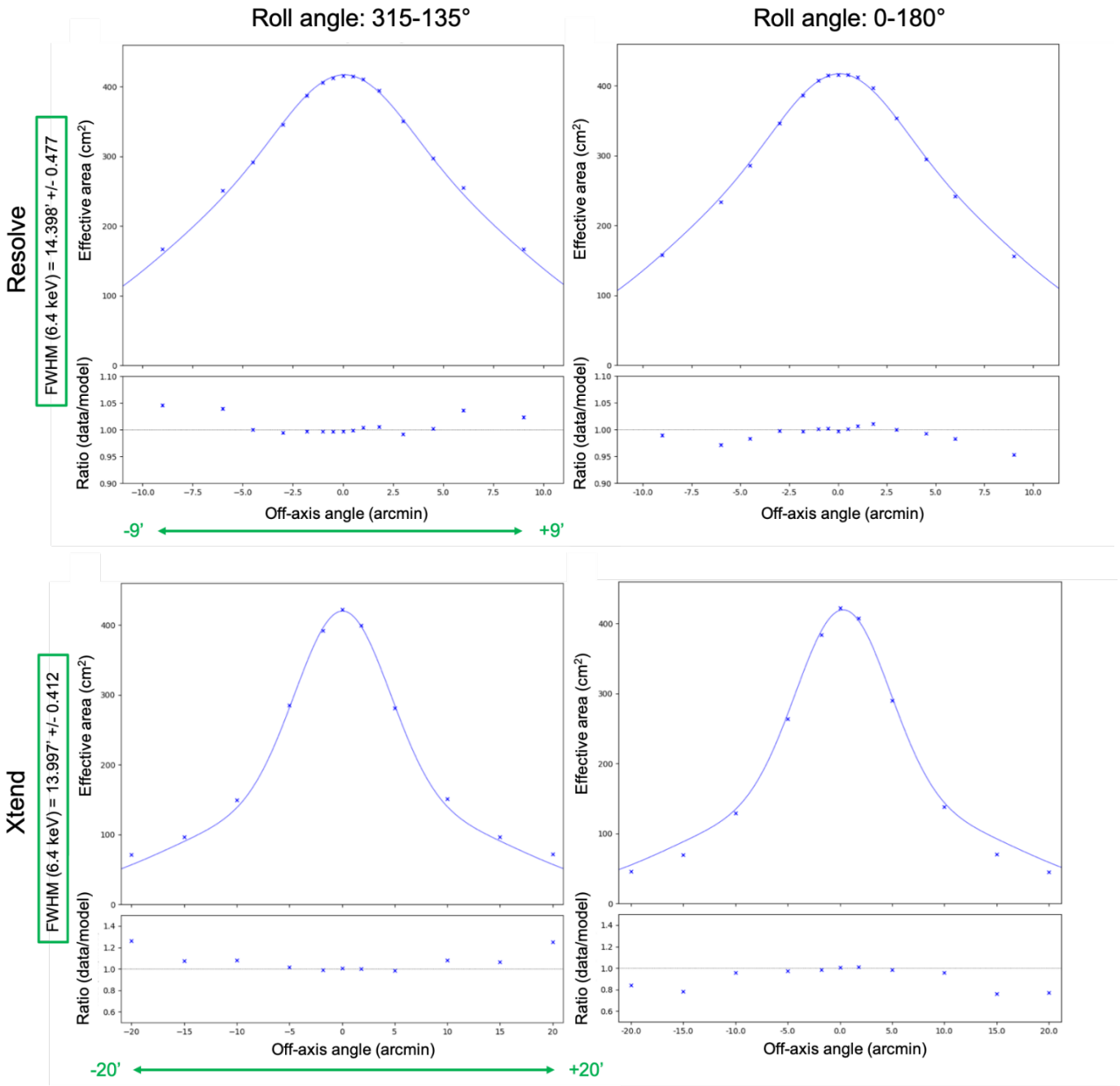

Figure 4: Measurements at 6.4 keV of the effective area (at E=6.4keV) and 2D fit, with projection in the directions defined by mirror roll angles 315 – 135° (centered on the mirror quadrants, left panel) and 0 -180° (along the quadrants boundaries, right panel), for Resolve (top panel) and Xtend (bottom panel) XMAs. The FoVs (i.e. FWHM) derived from the 2D fits at 6.4 keV are given for both XMAs.

2.1.2 Field of View

As explained in the previous paragraph, we performed a 2D symmetric fitting of the vignetting curves, in order to get a unique value of the FoV in all directions (described in Figure 1) for each energy. We thus derived the FoV (i.e. the FWHM) from the 2D fits to vignetting curves for each measured energy, by calculating the width of the fitted combined model at half of its maximum value. We then performed a fit of the FoV as a function of the energy, using a combination of a Fermi function, a linear function, and a constant, as shown by the equation below:

$$FoV\ (E) = \frac{N}{e^{\beta\,(E-\mu)} + 1} + L \times E + C$$

Equation 1: Model used to fit the FoV as a function of energy

This model is a phenomenological model, used to interpolate the FoV between measured energies. It has been chosen to fit the data based on the shape of the distribution of FoV as a function of energy, and was already representing well Hitomi's ground calibration data.

2.2 Results

The variation of the FWHM of the FoV (derived from the 2D modeling of the vignetting curves for both Resolve and Xtend XMAs), as a function of energy, is well fitted with the function described in Equation 1, as measurements and models differ by less than 5%. The values of the corresponding parameters of these fits (see Equation 1) were provided to the SDC in a first delivery, and then incorporated in the CalDB file. This vignetting coefficients CalDB fits file contains two lines (one for each instrument) in its main extension, with the fitted parameters from the modeling of the FoV as a function of energy, using the following notation: *PAR0* corresponds to N in Equation 1, *PAR1* is β, *PAR2* is μ, *PAR3* is L, and *PAR4* is C.

2.3 Final remarks

The XRISM and Heasoft software that previously used a Hitomi-version of the vignetting coefficients CalDB file requires a complete characterization of the vignetting functions, which is provided by the 2D modeling of the XRISM data explained above. However, the current version of the software is based on implementing less sophisticated 1D modeling. Therefore, this CalDB delivery will be superseded by the subsequent delivery, in which the coefficients will be compatible with the current XRISM software (see Section 3).

3 Revision - CalDB Release 20230815

CalDB Filename	Validity date	File(s) as delivered	Delivery date	Comment
xa_gen_vigncoef_20190101v002.fits	20190101 00:00 UT	FoV_fit_update20230901.pdf	20230902	Updated modeling of the vignetting curves, and hence of the FWHM of the FoV

3.1 Data Analysis

For the second delivery, we re-analyzed the data in a different way from the one used for the first delivery, in order to be compatible with the existing version of the software.

3.1.1 Vignetting Curves

Instead of using a 2D model combining a Gaussian and a Lorentzian component, we fitted this time the effective area as a function of the off-axis angle, for each energy, in each direction described in Figure 1, with a 1D single Lorentzian model, to match the definition of the vignetting curve used in the software. Figure 5 below shows the vignetting curves at all energies and in the four directions defined by the mirror roll angles, modeled by a Lorentzian function, for Resolve. As shown by the ratios of measurements over the fitted model, for Resolve, the vignetting functions modeled by a Lorentzian component agree with the ground data within 5% at all energies in the 1.5-11.1 keV range, and within +/-9′ of the Resolve optical axis.

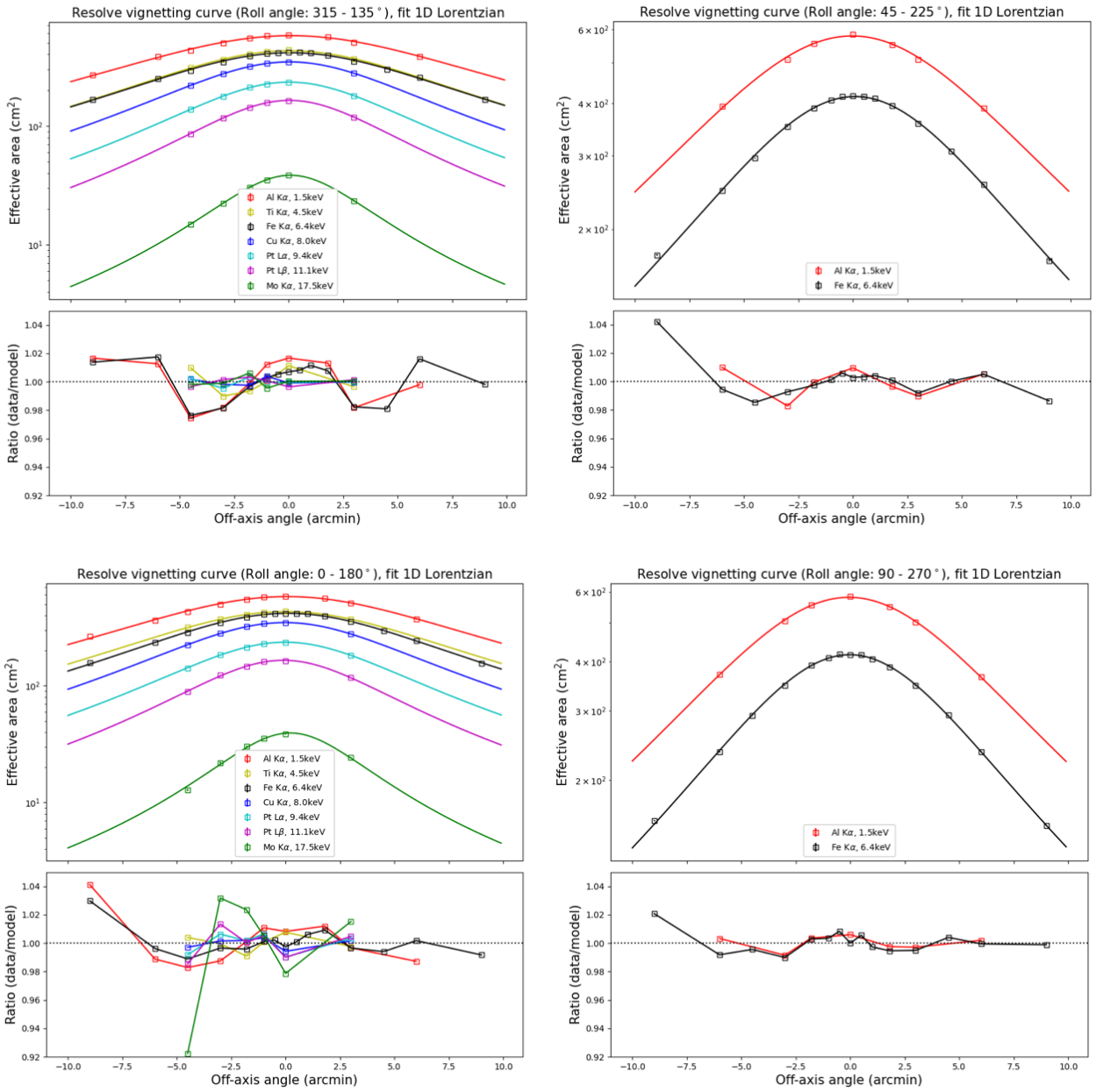

Figure 5: Resolve's vignetting curves in different directions (see Figure 1), for each energy, fitted in 1D with a single Lorentzian model. The bottom panels of each plot show the ratio of measurements over the fitted model.

We performed the same modeling for the Xtend vignetting curves. However, the simple Lorentzian model does not match the data as well as for Resolve, because of the larger range of off-axis angles, as shown for example in Figure 6.

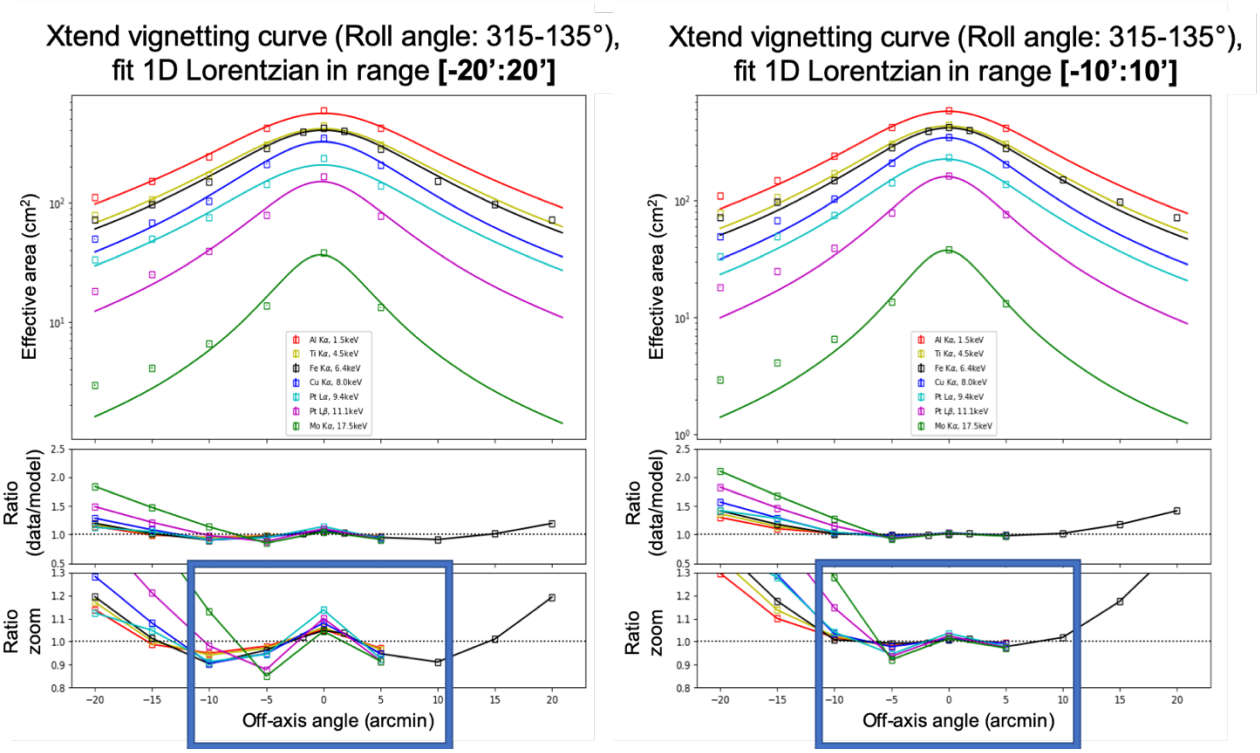

Figure 6: Xtend's vignetting curves in the direction of the mirror roll angles 315-135° (centered on the XMA's quadrants), for each energy, fitted in 1D with a single Lorentzian model. On the left panel, the fit is performed on the full range of off-axis angles, i.e. between -20′ and 20′. On the right panel, the fit is restricted to the data inside the range of off-axis angles from -10′ to 10′. The two bottom panels of each plot show the ratio of measurements over the fitted model, with different vertical scales. The blue boxes highlight the difference between both fitting methods, in the -10′ to 10′ range.

On the left panel of Figure 6, the fit of Xtend data is performed on the full range of off-axis angles, from -20′ to 20′. The ratio of measurements over the model shows that the fit around the optical axis poorly matches the data, with a discrepancy of up to 14% for energies from 1.5-9.4 keV between -10′ and 10′. In order to get a more accurate value of the width of the vignetting curve, i.e. a better estimation of the FoV of Xtend XMA, we restrained the fit in the range of off-axis angles between -10′ to 10′. Such a fit allows a better match with the data around the optical axis, as shown by the ratio on the right panel of Figure 6, with a discrepancy improved to only 6% for energies from 1.5-9.4 keV between -10′ and 10′. However, note that at higher energy, the fit is slightly worse in this restricted range of off-axis angles (e.g. the discrepancy between the model and the data increases from 12% to 15% at 11.1keV). Even if the model does not match the data as well on the tails of the vignetting curve, it generally describes better the core of the vignetting function, so the estimates of the centers and the widths are more accurate when fitting the Xtend data between -10′ and 10′. Figure 7 below shows the vignetting functions of Xtend, in all energies and all directions, fitted with a 1D Lorentzian model, in the restricted off-axis angle range of [-10′:10′].

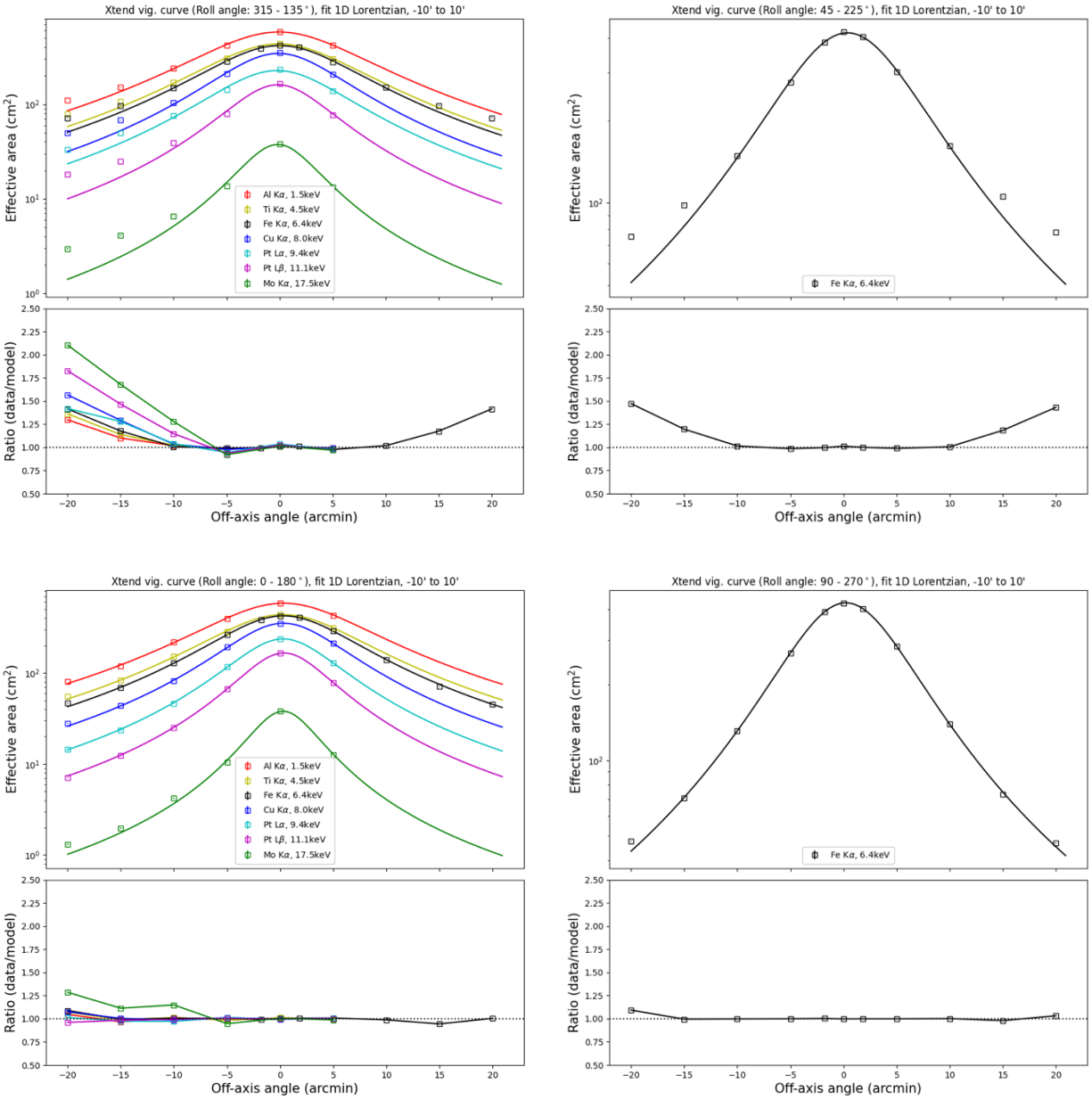

Figure 7: Xtend's vignetting curves in different directions (see Figure 1), for each energy, fitted in 1D with a single Lorentzian model, between off-axis angles -10′ and 10′. The bottom panels of each plot show the ratio of measurements over the fitted model.

As shown by the ratios of Figure 7, for Xtend, the fits are good to better than 6% at energies up to 9.4 keV, within +/- 10′ of the Xtend optical axis. Above 9.4 keV, the deviation can exceed 25%. Outside of the +/- 15′ range, the deviation between data and model is at least 10% for all the energies used and is as much as 82% at 11.1 keV.

3.1.2 Field of View

As explained in the previous paragraph 3.1.1, for the second delivery, we performed a 1D fitting of the vignetting curves, in each direction described in Figure 1, with a single Lorentzian model, and we calculated the average value of the FHWM (i.e. the width of the Lorentzian model) in all the directions, to get a unique value of the FoV for each measured energy. We then performed a fit of the FoV as a function of the energy, using the same function as for the first delivery, described by Equation 1 (see paragraph 2.2.2).

3.2 Results

Figure 8 shows the measured FoV (i.e. FWHM) from the 1D fitting with a Lorentzian model, for both Resolve and Xtend XMAs, as a function of energy, fitted with the function described in Equation 1. The ratio of measurements over the model is plotted in the lower panel and shows that the dependence of the FoV on the energy is well represented by this model, as measurements and models differ by less than 10%.

The corresponding parameters of these fits (see Equation 1) were provided to the SDC in a second delivery, as presented in Table 1 below, and then incorporated in the CalDB file. The parameters are very similar between both XMAs. We note that the β parameter is poorly constrained. As this parameter affects the slope of the break around 8 keV in the curve shown in Figure 8, we applied a high limit to this parameter during the fit, to get a smoother and thus more realistic curve to model the FoV as a function of the energy.

Table 1: CalDB parameters for the modeling of the FoV (derived from the 1D fitting of the vignetting curves with a Lorentzian model) as a function of energy, for both XMAs (see Equation 1). Note that in the CalDB file, N corresponds to PAR0, β is PAR1, μ is PAR2, L is PAR3, and C is PAR4.

	Resolve	Xtend
N (arcmin)	2.31 ± 1.13	2.20 ± 1.53
β (keV^{-1})	3.41 ± 19.17	3.50 ± 0.08
μ (keV)	7.78 ± 1.29	7.72 ± 1.41
L (arcmin keV^{-1})	-0.45 ± 0.09	-0.43 ± 0.13
C (arcmin)	14.85 ± 1.17	14.87 ± 1.80

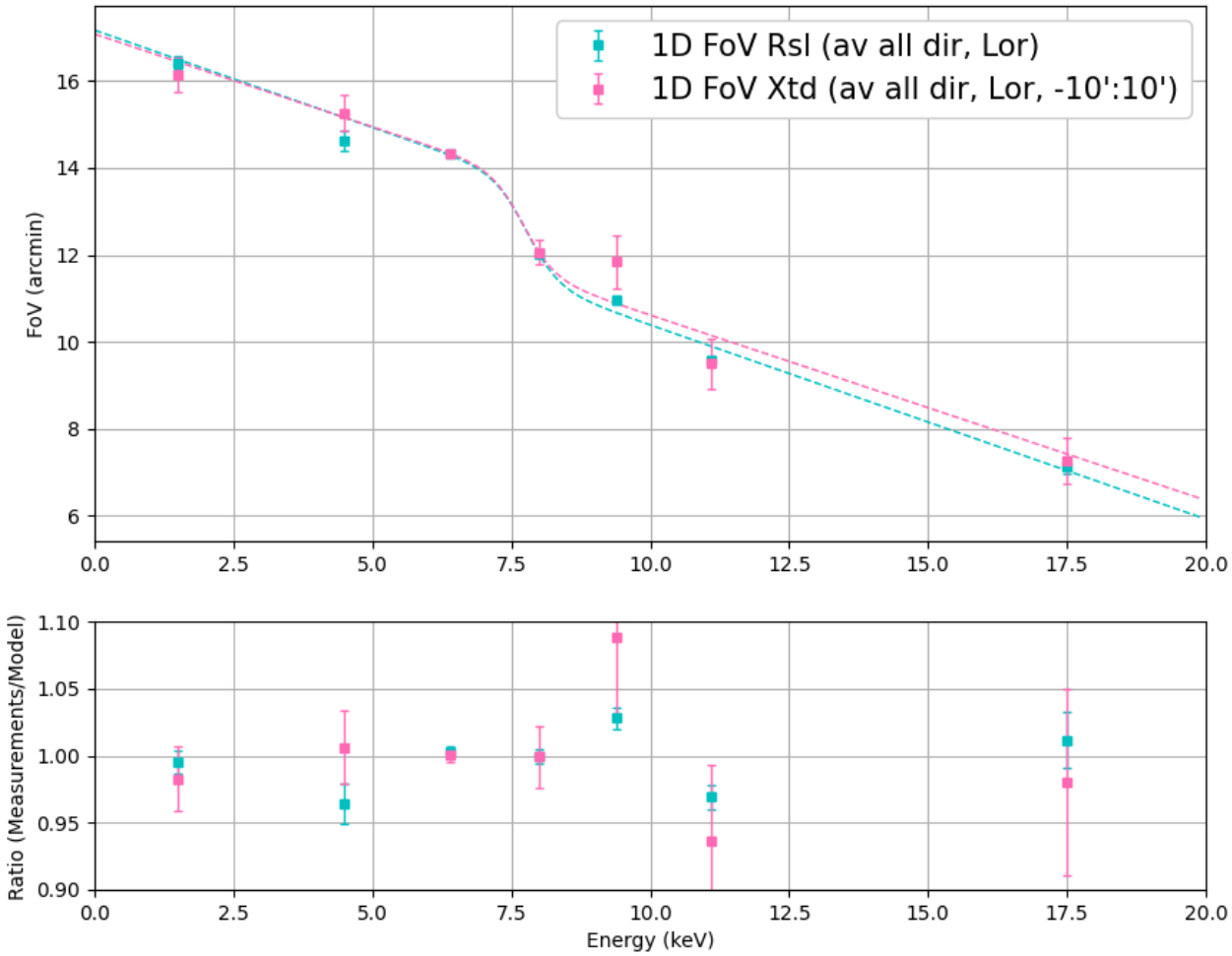

Figure 8: FoV as a function of the energy, for Resolve (cyan squares) and Xtend (pink squares). The top panel shows the measured FoV (derived from the 1D fitting of the data with a single Lorentzian model) as well as the fitted model (described by Equation 1) for both XMAs. The FoV is the average value of the FWHM in all directions. Note that these values are derived from the fit of the vignetting curves over the full range of off-axis angles for Resolve, while they come from the fit between -10′ and 10′ for Xtend, as described in the text. The bottom panel shows the ratio between these measurements and the corresponding fitted model.

3.3 Changes from previous versions

While we first used a 2D model combining a Gaussian and a Lorentzian component to fit the vignetting curves for the first delivery, we simply used a single 1D Lorentzian component for the revised delivery, to match the model defined in the software. Despite the difference between the models used in the two deliveries, the values of centers and FWHM of the vignetting curves are consistent within the error bars. Furthermore, the same model has been used to fit the FoV as a function of the energy for both deliveries, and the resulting parameters are also consistent within the error bars.

4 References

[1] XRISM Science Team, “XRISM Quick Reference,” arXiv e-prints, arXiv:2202.05399 (Feb. 2022); https://doi.org/10.48550/arXiv.2202.05399

[2] Rozenn Boissay-Malaquin, Takayuki Hayashi, Keisuke Tamura, Takashi Okajima, Toshiki Sato, Lawrence Olsen, Richard Koenecke, Wilson Lara, Leor Bleier, Megan E. Eckart, Maurice Leutenegger, Tahir Yaqoob, Meng Chiao, "Ground Calibration of the X-ray Mirror Assembly for the X-Ray Imaging and Spectroscopy Mission (XRISM) I - Measurement Setup and Effective Area," Proc. SPIE 12181, Space Telescopes and Instrumentation 2022: Ultraviolet to Gamma Ray, 121811U (31 August 2022); https://doi.org/10.1117/12.2627563

[3] Keisuke Tamura, Takayuki Hayashi, Rozenn Boissay-Malaquin, Takashi Okajima, Toshiki Sato, Lawrence Olsen, Richard Koenecke, Wilson Lara, Leor Bleier, Megan E. Eckart, Maurice Leutenegger, Tahir Yaqoob, Meng Chiao, "Ground Calibration of the X-ray Mirror Assembly for the X-Ray Imaging and Spectroscopy Mission (XRISM) II - Imaging Performance and Stray Light," Proc. SPIE 12181, Space Telescopes and Instrumentation 2022: Ultraviolet to Gamma Ray, 121811V (31 August 2022); https://doi.org/10.1117/12.2629534

[4] Takayuki Hayashi, Rozenn Boissay-Malaquin, Keisuke Tamura, Takashi Okajima, Toshiki Sato, Lawrence Olsen, Richard Koenecke, Wilson Lara, Leor Bleier, Maurice Leutenegger, Megan E. Eckart, Tahir Yaqoob, Meng Chiao, "Ground Calibration of the X-ray Mirror Assembly for the X-ray Imaging and Spectroscopy Mission (XRISM) III - Performance Variation across the Aperture," Proc. SPIE 12181, Space Telescopes and Instrumentation 2022: Ultraviolet to Gamma Ray, 121815Y (31 August 2022); https://doi.org/10.1117/12.2627975